Occlusal Caries Detection Using Random Walker Algorithm: a Graph Approach

Christos G. Bampis, Georgia D. Koutsouri, Elias Berdouses, Evanthia E. Tripoliti, *Member IEEE*, Dimitra Iliopoulou, Dimitrios Koutsouris, Constantine Oulis, and Dimitrios I. Fotiadis, *Senior Member IEEE*

***Abstract*— The aim of this work is to present a modification of the Random Walker algorithm for the segmentation of occlusal caries from photographic color images. The modification improves the detection and time execution performance of the classical Random Walker algorithm and also deals with the limitations and difficulties that the specific type of images impose to the algorithm. The proposed modification consists of eight steps: 1) definition of the seed points, 2) conversion of the image to gray scale, 3) application of watershed transformation, 4) computation of the centroid of each region, 5) construction of the graph, 6) application of the Random Walker algorithm, 7) smoothing and extraction of the perimeter of the regions of interest and 8) overlay of the results. The algorithm was evaluated using a set of 96 images where 339 areas of interest were manually segmented by an expert. The obtained segmentation accuracy is 93%.**

I. Introduction

Semi-automatic image segmentation methods gained the increased interest of researchers since they permit the targeted extraction of regions of interest particularly from difficult images [1-3]. Our focus on this work is a modification of a supervised segmentation algorithm called Random Walker (RW) and its application for the detection of occlusal caries.

The RW algorithm was presented by Leo Grady *et al.* [4]. It incorporates most of the key features of semi-automatic methods such as fast editing, arbitrary segmentation and robustness to noise. According to this algorithm, the image is treated as a weighted graph. The nodes of the graph correspond to pixels, while the edges connect similar nodes. This similarity is typically measured by a Gaussian weighting function. The segmentation is achieved by computing the probability of a random walker starting from an unlabeled node to reach a labeled node. The algorithm, through the weighting function, takes into consideration only information about the intensity of adjacent pixels (using a typical 4 or 8 pixel neighborhood), ignoring thus spatial features which can improve the resulting delineations.

Towards this direction Cui *et al.* [2] integrated into the classical RW algorithm spatial features. Spatial information is used to measure the spatial effects between pixels and is effectively combined with intensity information to define the weighted function. Sinop *et al.* [3] proposed a new seeded image segmentation algorithm by combining the Graph-Cuts algorithm [5] and the Random Walker algorithm [1]. The unification of the two above mentioned algorithms in one framework allows exploitation of the advantages of the two algorithms and diminishment of their limitations ("shortcutting" problem of Grap-Cut algorithm, no "tight" segmentations of Random Walker algorithm). Li *et al.* [6] aimed not only to improve the segmentation accuracy of the RW algorithm but also its computational time. In order to achieve this, the toboggan segmentation algorithm [7, 8] was applied as a preprocessing step prior to RW algorithm. According to this approach, the pixels of the image are locally classified based on textural features, a weighted graph is constructed using a gravity operator, reducing significantly the number of nodes, and then the RW algorithm is applied in order to resegment the image.

The proposed modification of RW algorithm improves the performance of the classical RW algorithm in terms of accuracy and execution time. It incorporates spatial information and applies the watershed segmentation algorithm [9, 10] as a preprocessing step which according to [11] produces the same results as the toboggan algorithm. The watershed segmentation is preferred due to its simplicity. The proposed modification is differentiated from those reported in the literature since it is applied adaptively to color images. More specifically, all the three color channels of the image are utilized and not only the grayscale values, avoiding thus any color information loss. Each channel of the image is regularized separately so that its contribution to the final weight function is proportionate to its value range. Additionally, in the proposed graph approach each node is related to a set of pixels rather than a single pixel, decreasing thus the execution time of the algorithm for large images where the traditional pixel based RW algorithm will take more time. The proposed modification is applied in order to segment occlusal caries, an important medical problem due to the changing pattern of dental caries that has occurred in the last decades. Dental caries is an irreversible microbial disease of the calcified tissues of the teeth [12]. Occlusal caries represent the most

C. G. Bampis is with the School of Electrical and Computer Engineering, National Technical University of Athens, Athens Greece (e-mail: herc_christos@hotmail.com).

G. D. Koutsouri. D. Koutsouris, D. Iliopoulou are with Biomedical Engineering Laboratory, National Technical University of Athens, Greece (e-mail: tzwrtzia.k@gmail.com, dkoutsou@biomed.ntua.gr, dilio@biomed.ntua.gr).

E. Berdouses and C. Oulis are with the Dept. of Paediatric Dentistry, Dental School, National and Kapodistrian University of Athens, Greece (e-mail: eberd@enternet.gr, cjoulis@paedoclinic.gr). E. E. Tripoliti and D. I. Fotiadis are with the Unit of Medical Technology and Intelligent Information Systems, Dept. of Materials Science and Engineering, University of Ioannina, Greece (email: etripoliti@gamil.com, corresponding author to provide phone: +302651008803; fax: +302651007092 e-mail: fotiadis@cc.uoi.gr).

978-1-4244-7929-0/14/$26.00 ©2014 IEEE

common type of cavities (they represent 12.5% of all tooth surfaces, however, are the location of over 50% of all dental caries [13]). The diagnosis of occlusal caries may be expected to be fairly easy to diagnose since these surfaces are readily accessible for visual inspection. However, clinically or radiographically, diagnosis (detection and classification) of occlusal lesions is a delicate problem due the complicated morphology of the occlusal surface (complicated 3D space of the occlusal surfaces, incorporation of fossae and grouves, existence of a great range of variations).

The method was applied in 96 digital color images were 339 areas were annotated by an expert. The method was compared with its gray scale analog and both the methods were evaluated in terms of segmentation accuracy.

II. Materials and Methods

A. Dataset

We have collected 96 digital color images (10 *in vivo* and 86 *in vitro* images). The images were collected in the School of Dentistry of the National Kapodistrian University of Athens. The *in vivo* images were recorded using a Canon Rebel XTi 10.1 MP digital camera, with lense Canon Macro EF 100mm 1:2.8 USM, flash Macro Ring Light MR14 EX and magnification 1:1. The *in vitro* images were recorded using the Olympus E-500 Digital 8MP camera with lense Olympus digital 50mm macro and an Olympus 2x Teleconverter (EC-20) giving a magnification almost 1:2. The speed was set at 1/125sec and diaphragm at F45 stop at 0.79m focusing distance. The ring flash is a Starblitz (Macrolite-1000 Auto) [14].

The images were annotated by one expert. The expert outlined the perimeter of the decalcification (DA) and occlusal caries areas (OC) using a software developed in MATLAB v7.12. The expert picks the pixels that constitute the perimeter of the regions of interest. Once the selection of the pixels is completed, the border of the polygonal region of interest is created within the image. For this purpose the *roipoly* Matlab function is utilized. It displays the image on the screen and lets the user specify the polygon using the mouse. Once the selection of points is completed, it draws the selected polygon on the image [15]. In the dataset 339 regions of interest were identified.

B. The supervised method

The proposed method consists of eight steps. First, the user defines the seeds in the foreground and background of the image. Then (second step), the image is converted to gray scale and the raw watershed transform is applied so that the image is over-segmented (third step). Each region of the image is represented by a node (centroid of the region) (fourth step). The nodes are centered spatially in each region and its intensity value is a vector containing the mean values of the corresponding pixel intensities of each color channel in the RGB (Red, Green, and Blue) color space. The computation of the centroids for each region, produced by the watershed transform, leads to the construction of the graph (fifth step). In the sixth step the RW algorithm is applied using the set of seed pixels that were defined in the first step and they have a predefined label. If a two class segmentation problem is considered, the label 1 is arbitrarily set for a pixel belonging to the region of interest and the label 0 for a pixel belonging to the background. As a result, all pixels belonging in this node's region are labeled accordingly. Finally, the perimeters of the located regions are extracted and smoothed (seventh step) and overlay of the results takes place (eighth step).

Step 1: Definition of seed points

In the first step the user is asked to select initial seed points in the region of interest (foreground) and in the background of the image. The seed points are accompanied by the corresponding label, depending on the region they belong to. For low contrast images an increased number of foreground seeds is needed so that weak edges can be properly identified. Thus, the number of seed points is adjusted depending on the type of the region of interest. In practice, 2-3 seeds are adequate for intense regions and 18-20 seeds for low contrast ones. The number of background seeds is tuned accordingly to 20-25 seeds and 40-45 seeds, respectively.

Step 2: Conversion of the image to gray scale

The color image is converted to gray scale intensity image (Im) by eliminating the hue and saturation information while retaining the luminance. More specifically, the RGB values are converted to grayscale values by forming a weighted sum of the R , G and B components using the following formula [16]:

$$Im(x,y) = 0.2989 * R + 0.5870 * G + 0.1140 * B , \quad (1)$$

where R , G and B are the intensity values of the red, green and blue channel, respectively, for a pixel located in (x,y).

Step 3: Application of watershed transform

The watershed transform is applied so that the image is over-segmented. The value of the intensity (e.g. of the gradient image) is assumed to be the elevation information. Pixels having the highest gradient magnitude intensities correspond to watershed lines, which represent the region boundaries. Water 'placed' on any pixel enclosed by a common watershed line flows downhill to a common local intensity minimum. Pixels draining to a common minimum form a catch basin, which represents a region [10].

Step 4: Computation of the centroids of each region

For each region R_j, $j = 1,...,M$ extracted from the watershed transformation the spatial centroid is computed using the following formula:

$$h_j = \begin{pmatrix} \mu_{j1} \\ \mu_{j2} \end{pmatrix}, \quad (2)$$

where μ_{j1} and μ_{j2} are given by:

$$\mu_{j1} = \frac{1}{N_j} \sum_{i=1}^{N_j} x_i \,, \tag{3}$$

and

$$\mu_{j2} = \frac{1}{N_j} \sum_{i=1}^{N_j} y_i \,, \tag{4}$$

respectively. x and y represent the spatial coordinates for pixel i, M denotes the number of regions, and N_j denotes the number of pixels belonging to region j [6].

Step 5: Construction of the graph

For the construction of the graph $G(E,V)$, where E is the set of edges of the graph and V the set of the nodes of the graph the following formulas are utilized. Equation (2) is used for the determination of the nodes, while the weight of the edges between the nodes is assigned as:

$$w_{i,j} = \begin{cases} e^{-\beta \left\| g_i - g_j \right\|^2 - \left\| h_i - h_j \right\|^2} & if\ R_i \sim R_j \\ 0 & otherwise \end{cases}. \tag{5}$$

The parameter β denotes the free parameter of the algorithm, g_i denotes the mean intensity of all pixels belonging in the region R_i and the symbol ~ denotes that regions i and j are adjacent [3, 6]. The value of parameter β is set equal to 100, a value commonly selected in the literature.

Step 6: Application of the RW algorithm

The RW algorithm is applied and the labels for each unlabeled node are determined. The main idea underlying the RW algorithm is to determine the probability that a random walker starting from an unlabeled node reaches a labeled node, given some definition of the probability of stepping from a given node to each neighbor. Each unlabeled node is then assigned a label with respect to the maximum between the foreground seeds' transition probabilities and the background seeds' ones. These transition probabilities between the nodes are determined using the edge weights as described in (5) [3].

Step 7: Extraction of the perimeter

After computing the labels for each node, the same label (0 or 1) is assigned to all pixels belonging to the corresponding region. Since there are pixels lying in the cut lines produced by the watershed transformation, a distinction is made between those pixels that are adjacent to pixels belonging to both types of regions (foreground or background) and those that are adjacent to only one type of region. For the first case a background label is assigned whereas in the second case the label is selected with respect to the region which is adjacent to these pixels.

Step 8: Overlay of the results

In the eighth step the foreground masks are extracted and the segmented perimeters for regions of interest are overlaid in the initial image and the final segmented image is created.

III. RESULTS

The proposed method was evaluated using the dataset described in Section II.A. This method is compared with its grayscale analog where we make use of the grayscale color values only, whereas all other steps are the same (RW-gray). The RW-gray algorithm was also evaluated in the same dataset and it was compared, in terms of quantity and quality, with the proposed method. The two methods are applied to each one of the 96 images and the regions of interest (occlusal caries and decalcification areas) are segmented.

The results are depicted in Table I and in Fig. 1. The accuracy is computed in terms of pixels. This is achieved by comparing the pixels detected by the method (RW-gray and/or proposed RW) with the pixels, which according to the annotation of the expert belong to the region of interest.

TABLE I. COMPARISON OF THE PROPOSED METHOD WITH THE RW-GRAY ALGORITHM

Measure	**Method**	
	RW-gray	***Proposed RW***
Accuracy	91,66%	92,60%

The accuracy reported on Table I can lead to the conclusion that the two methods are almost equivalent (1% difference). However, the quality of the segmentation is significantly different between the two methods. This is depicted in Fig. 2 where the segmentation results of the RW-gray algorithm, of the proposed method and the corresponding results of manual segmentation are presented. The yellow dots correspond to background seeds, while the green dots to foreground seeds. The green perimeter depicts the annotation of the expert, while the red and the blue depict the segmentation results of the RW-gray and proposed RW algorithm, respectively. The region indicated by the orange arrow reflects the fact mentioned above since the RW-gray algorithm merges two of the regions annotated by the expert and covers large area of the healthy tooth.

The results of both the methods are affected (positively or negatively) by the position and the number of seeds in the image and consequently by the expertise of the user. This is presented in Fig. 3. More specifically, in Fig. 3(a) the seeds are located in the center of the large region annotated by the doctor (orange arrow) and as a consequence both versions of the RW algorithm could not detect the "edges" of the specific region. By modifying the distribution and the number of the foreground seeds the segmentation results presented in Fig. 3(b) are produced. Although the above mentioned lost areas of the region are detected, the quality of the results is not satisfactory. By changing both the distribution and the number of foreground and background seeds the results are improved as it is depicted in Fig. 3(c).

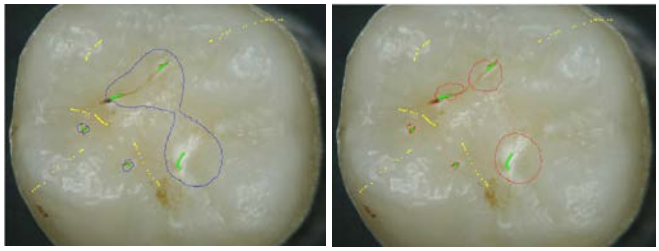

(a) Segmentation results of the RW-gray algorithm.

(b) Segmentation results of the proposed – RW algorithm.

(c) Annotation by the expert.

Figure 1. Segmentation results of the two versions of the RW algorithm (red line: RW-gray, blue line: Proposed RW) *vs.* annotation of the expert (green line).

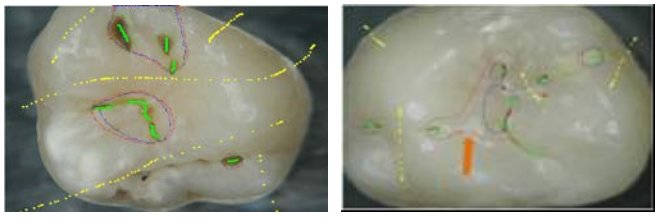

(a) Same quality of segmentation results.

(b) Different quality of segmentation results.

Figure 2. Segmentation results of the two versions of the RW algorithm (red line: RW-gray, blue line: Proposed RW) .

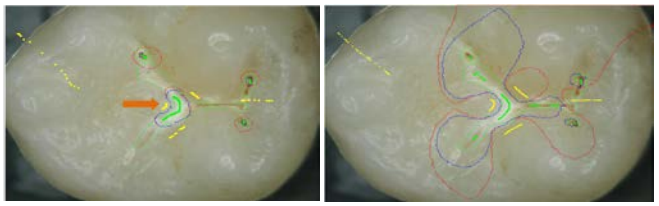

(a) Initial distribution.

(b) Distribution with negative effect on the segmentation results.

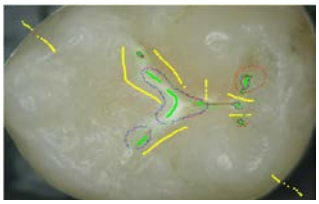

(c) Distribution with positive effect on the segmentation results.

Figure 3. Segmentation results depending on the position and number of the seeds (red line: RW-gray, blue line: Proposed RW) .

IV. Conclusions

A modification of the RW algorithm was presented. The proposed modification incorporates color from all channels and spatial information and exploits the employment of the watershed transform to improve the segmentation accuracy and the execution time of the standard RW algorithm, which takes more than an hour to run in an image. It is adaptively applied and evaluated in a dataset of 96 color digital images depicting DA and OC areas. The performance of the method is affected by the initial selection of foreground and background seeds point, an issue that will be addressed in our future work.

References

[1] Leo Grady, "Random Walks for Image Segmentation," *IEEE Trans. on Pattern Analysis and Machine Intelligence*, vol. 28, no. 11, pp.1768-1783, Nov. 2006.

[2] Z. Cui, W. Li, G. Pan, L. Gao, "An Improved Random Walker using Spatial Feature for Image Segmentation," in *Proc. of 25th Chinese Control and Decision Conference (CCDC)*, Guiyang, 2013, pp.1479-1482.

[3] A. K. Sinop, L. Grady, "A Seeded Image Segmentation Framework Unifying Graph Cuts and Random Walker Which Yields a New Algorithm," in *Proc. of 11th IEEE International Conference on Computer Vision,* Brazil, 2007, pp. 1-4.

[4] L. Grady, G. Funka-Lea, "Multi-label image segmentation for medical applications based on graph-theoretic electrical potentials," in *Proc. of Computer Vision and Mathematical Methods in Medical and Biomedical Image Analysis*, Prague, 2004, pp. 230-245.

[5] Y. Boykov, G. Funka-Lea, "Graph-cuts and efficient n-d image segmentation", *International Journal of Computer Vision*, vol. 70, no. 2, pp. 109-131, 2006.

[6] G. Li, L. Qingsheng, C. Jian, "A New Fast Random Walk Segmentation Algorithm", in *Proc. of 2nd International Symposium on Intelligent Information Technology Application*, Shanghai, 2008, pp. 693-697.

[7] J. Fairfield, "Toboggan Contrast Enhancement for Contrast Segmentation," in *Proc. of 10th IEEE International Conference on Pattern Recognition*, 1990, pp. 712-716.

[8] X. Yao, Y. P. Hung, "Fast Image Segmentation by Sliding in the Derivative Terrain", in *SPIE Proc. of Intelligent Robots and Computer Vision X: Algorithms and Techniques*, 1991, pp. 369-379.

[9] A. N. Evans, "Morphological gradient operators for color images," in *Proc. of IEEE International Conference on Image Processing*, 2004, pp. 3089-3092.

[10] S. Beucher, "Watersheds of functions and picture segmentation," in *Proc. of IEEE International Conference of Acoustic, Speech, Signal Processing*, 1982, pp. 1928–1931.

[11] Y.C. Li, Y.P. Tsai, Y.P. Hung, Z.C. Shih, "Comparison between immersion-based and toboggan-based watershed image segmentation," *IEEE Transactions on Image Processing*, vol.15, no.3, pp.632 – 640, 2006.

[12] G. Sarode, A. Shelar, S. Sarode, N. Bagul, "Association between Dental Caries and Lipid Peroxidation in Saliva‖," *International Journal of Oral & Maxillofacial Pathology*, vol. 3, no. 2, pp.02-04, 2012.

[13] R. Welbury, M. Raadal, N.A. Lygidakis, "EAPD guidelines for the use of pit and fissure sealants‖," *European Journal of Paediatric Dentistry*, vol. 3, pp. 179-186, 2004.

[14] G. D. Koutsouri, E.Berdouses, E. E. Tripoliti, C. Oulis, D. I. Fotiadis, "Detection of occlusal caries based on digital image processing," *Proc. of the 13th IEEE International Conference on BioInformatics and BioEngineering, 2013.*

[15] R. C. Gonzalez, R. E. Woods, S. L. Eddins, Digital Image Processing Using Matlab, Gatesmark Publishing, 2009.

[16] R. M. Haralick, L.G. Shapiro, Computer and Robot Vision, Addison-Wesley, pp: 28-48, 1992.